Mon. Not. R. Astron. Soc. **000**, 000–000 (2001) Printed 1 February 2008 (MN LATEX style file v1.4)

Virial masses of galactic halos from galaxy-galaxy lensing: theoretical modeling and application to SDSS

Jacek Guzik[1,2] & Uroš Seljak[1]
[1] *Department of Physics, Jadwin Hall, Princeton University, Princeton, NJ 08544*
[2] *Astronomical Observatory, Jagiellonian University, Orla 171, 30-244 Kraków, Poland*

1 February 2008

ABSTRACT
We present a theoretical analysis of galaxy-galaxy lensing in the context of halo models with CDM motivated dark matter profiles. The model enables us to separate between the central galactic and noncentral group/cluster contributions. We apply the model to the recent SDSS measurements with known redshifts and luminosities of the lenses. This allows one to accurately model the mass distribution of a local galaxy population around and above $L_\star$. We find that virial mass of $L_\star$ galaxy is $M_{200} = (5-10) \times 10^{11} h^{-1} M_\odot$ depending on the color of the galaxy. This value varies significantly with galaxy morphology with $M_\star$ for late types being a factor of 10 lower in u', 7 in g' and a factor of 2.5-3 lower in r', i' and z' relative to early types. Fraction of noncentral galaxies in groups and clusters is estimated to be below 10% for late types and around 30% for early types. Using the luminosity dependence of the signal we find that for early types the virial halo mass M scales with luminosity as $M \propto L^{1.4\pm0.2}$ in red bands above $L_\star$. This shows that the virial mass to light ratio is increasing with luminosity for galaxies above $L_\star$, as predicted by theoretical models. The virial mass to light ratio in i' band is $17(45) h M_\odot/L_\odot$ at $L_\star$ for late (early) types. Combining this result with cosmological baryon fraction one finds that $70(25)\% h^{-1} \Upsilon_i \Omega_m/12\Omega_b$ of baryons within r_{200} are converted to stars at $L_\star$, where Υ_i is the stellar mass to light ratio in i' band. This indicates that both for early and late type galaxies around $L_\star$ a significant fraction of all the baryons in the halo is transformed into stars.

1 INTRODUCTION

Weak lensing by matter along the line of sight between the source and the observer shears the images of the background galaxies, inducing ellipticity distortions (see Bartelmann & Schneider 2001 for a review of weak lensing). Although away from rich clusters the effect is too small to be detectable for individual galaxy lenses, it can be measured statistically as a function of relative separation from the galaxy. This requires averaging over the tangential ellipticities of all the background galaxies relative to the lens and over all the lenses (galaxies which are in the foreground). Until recently this averaging, named galaxy-galaxy (g-g) lensing, was done as a function of apparent angular position in the sky (Tyson et al. 1984, Brainerd, Blandford, & Smail 1996, Hudson et al. 1998, Fischer et al. 2000, Smith et al. 2001), so a signal at a given angular separation could be either coming from a small radial distance of a nearby lens or from a large distance of a far lens. This made the theoretical interpretation of the data rather involved. First attempt to use distances was by Wilson et al. (2001), which however only had limited photometric information and so could only obtain reliable distances to early type galaxies.

Recent study of galaxy-galaxy lensing by SDSS collaboration (McKay et al. 2001) is a significant step forward in the study of galaxy-galaxy lensing. The spectroscopic sample of more than 35,000 lensing galaxies and 3.6 million background galaxies is large enough to allow one a detailed study of the relation between mass and light for several luminosity bands and morphological types. Since the distances for lens galaxies are known one can study the strength of the signal as a function of proper radial separation from the lens. In addition, because the survey is shallow, the redshift distribution of background galaxies is known from the deeper spectroscopic surveys (e.g. Lilly et al. 1995). In combination with above this means that the mean critical density is known for every lens, so one can average over the proper projected mass density rather than the shear itself. This fact greatly simplifies the theoretical analysis, since one can now measure the actual projected density as a function of galaxy luminosity and proper radial transverse distance from the galaxy. In addition, since the lens sample is at low redshift (mean $\bar{z} \sim 0.1$) redshift evolution is small and k-corrections are relatively reliable in red bands, further simplifying the theoretical interpretation.

In this paper we want to connect the SDSS observational results to the theoretical models in the context of our current understanding of galaxy formation models within the CDM paradigm. We will model the dark matter halos with CDM type of halo profiles (NFW profile; Navarro, Frenk, & White 1997), where the slope is gradually changing

from the inner slope between -1 to -1.5 to the outer slope of -3. Although other profiles have been proposed that differ significantly from NFW in the inner parts of the halo, they agree well with NFW in the outer parts (Klypin et al. 2001). NFW profile should be contrasted to the truncated singular isothermal sphere with a constant slope -2 out to a fixed radius which was often used used in the past work on g-g lensing. Our main goal is to determine the virial mass of the halo and its relation to the luminosity of the galaxy. This is important for theoretical models of galaxy formation, since it is usually assumed that only baryons within the virial radius are able to condense and form stars. By determining the virial mass for a given galaxy luminosity one can thus directly determine the efficiency of star formation in typical galactic halos. Luminosity dependence of the galaxy-galaxy lensing signal allows one to determine this as a function of halo mass, while morphology subsamples can determine it as a function of morphological type. By comparing the radial dependence of the signal with the theoretical models one can also determine the fraction of galaxies that live in larger halos such as groups and clusters. This is another parameter that can distinguish between the different galaxy formation models. Finally, comparison of high density sample to the field sample allows one to study the effects of dense enviroments, such as tidal stripping, on the dark matter profile and mass to light ratios. Thus g-g lensing allows one to make detailed tests of the galaxy formation models (e.g. Kauffmann et al. 1999, Benson et al. 2000, Somerville & Primack 1999). In principle g-g lensing can also allow a direct determination of the dark matter halo profile, although as we will show here at present the data do not have enough power to strongly constrain this.

An important issue in the theoretical analysis of g-g lensing is how to separate the contribution from the individual halo of the galaxy from that of the neighbouring galaxies or larger mass concentrations such as groups and clusters. The former should dominate on small scales while the latter on large scales. Previous work used the additional information obtained from the galaxy clustering to remove this contribution, but in general such analysis relies on the assumption that all the mass is associated with galaxies, which is invalid on scales where groups and clusters become dominant. Most of the mass in these systems is in a diffuse form and only about 5-10% is expected to be attached to individual galaxies (e.g. Springel et al. 2001, Ghigna et al. 2000, Bullock et al. 2001). This means that these systems cannot be modeled using the galaxies as the mass tracers, which only accounts for a small fraction of the total mass. In fact, theoretical models presented in this paper suggest the contribution from these group and cluster halos dominates the signal on scales above $200h^{-1}$kpc (see also Seljak 2000) and has to be carefully modeled to account for it.

Given that corrections to the profile on large scales are difficult to determine from the data directly one has to turn to theory for guidance. Realistic theoretical modeling of g-g lensing must combine galaxy formation models and dark matter models. One way is to use semi-analytic or hydrodynamic models of galaxy formation and combine them with N-body simulations (Guzik & Seljak 2001; White, Hernquist, & Springel 2001). This has the advantage of having a realistic distribution of dark matter and galaxies, but suffers from the lack of force and mass resolution. In addition, this approach by itself does not allow for a fast exploration of parameter space. The alternative approach is to use the recently popularized halo model applied to galaxies (Seljak 2000, Peacock & Smith 2000, Scoccimarro et al. 2001, Berlind & Weinberg 2001), which takes into account both the individual halo profiles (for galaxies either at the centers of the galactic halos or distributed within larger groups and clusters with a specified radial distribution) and correlations between the galaxies. This approach applied to the galaxy-dark matter correlations (which fully determines the g-g lensing signal) was shown to give the same results as the simulations in the regime of applicability (Seljak 2000). However, halo model is analytical, does not suffer from the resolution issues and provides a more physical interpretation of the results. Thus one can parametrize the model with the quantities one wishes to extract from the data and determine these directly. It also allows for a rapid exploration of the parameter space without the need to rerun cosmological simulations or to repopulate the halos with galaxies using semi-analytic galaxy formation models. In this sense the halo model provides a natural link between the observations and the theoretical models of galaxy formation.

Even though we will use the halo model to analyze g-g lensing the main features can be understood without it. Particularly robust conclusions are possible using the low density sample, where the clustering and group/cluster contribution can be neglected. In this case the signal can be taken simply as a projected radial mass profile of the halo averaged over the mass distribution of the halos determined by the galaxy sample. For the full and high density sample the contribution from groups and clusters can no longer be neglected, as it dominates the signal on scales above $200h^{-1}$kpc. This allows one to determine the fraction of galaxies in groups and clusters as well.

The outline of this paper is as follows: in section §2 we review the basic theory and halo model as applied to g-g lensing. In §3 we discuss the influence of the parameters introduced on the observed g-g lensing signal. We focus on the relative contributions to g-g lensing from galaxy, group/cluster and clustering terms and explore which parameters the observations are most sensitive to. In §4 we apply the model to the data to determine several of the model parameters. Interpretation of the results and conclusions are presented in §5.

2 CONTRIBUTIONS TO G-G LENSING FROM THE HALO MODEL

In the halo model it is assumed the galaxies form in collapsed dark matter halos. The halos are clustered among themselves and have a specified density profile. The contribution to g-g lensing comes either from the dark matter profile of the halo the galaxy is sitting in (one-halo or Poisson term) or from the clustering of all the other halos around a given galaxy (halo-halo term). As we show below the second contribution is small compared to the first one on scales below $1h^{-1}$Mpc of interest here. The one-halo term has two contributions. First is from the dark matter around the galaxy itself that depends on the dark matter halo profile. Second is from the dark matter in groups and clusters the galaxy may belong to, but is not at their center. In the latter case one

must also specify the radial distribution of galaxies inside these halos. The simplest case is to assume it is the same as the radial distribution of the dark matter (see e.g. Hoekstra et al. 2001 for some justification in the case of observations and Ghigna et al. 2000, Springel et al. 2001 for the case of simulations).

The relative contribution from the two one-halo components depends on the fraction of galaxies residing in groups and clusters. In general this fraction varies with luminosity, type and other selection criteria. Particularly simple is the low density sample in SDSS data, which consists mostly of the field galaxies and where the group/cluster fraction is likely to be small. When this is not the case, as for example for the high density selected sample or early type sample, one must also address the question of whether the halo profiles around galaxies that are within larger halos differ from the profile of equal luminosity galaxies in the field. Even if the galaxies that end up in groups and clusters do not have different star formation efficiencies, so that their luminosity is a good indication of the halo mass, they may still loose some dark matter after merging. This depends on the amout of tidal stripping, which itself depends on the radial orbit of the galaxy. Simulations indicate that the tidal radius should be defined at the orbit pericenter, which is the point of the closest approach to the center of the cluster (Ghigna et al. 2000). Since the orbits are very eccentric (typical ratios 1:5) the pericenter can be significantly smaller than the instantaneous galaxy position. Still, these simulations indicate that the halo profiles of most of the halos within halos remain unaffected out to where the density of the larger halo matches that of the smaller halo (Ghigna et al. 2000). Since it is the radial halo profile that is relevant for g-g lensing we will model the galaxies within clusters as a superposition of a smooth cluster profile (weighted by the radial distribution of galaxies) and an individual galactic halo profile, which is assumed to be the same as for the equal luminosity galaxy in the field. We discuss further below how this assumption can be tested with g-g lensing itself. We do not need to model the transition from the subhalo to the cluster, where there may be departures from this simple model, since one is observing a projected density with g-g lensing. Given that clusters are significantly larger than galactic halos the cluster dominates the signal at radii smaller than the 3-d transition point.

2.1 Theory

We are interested in the distribution of the dark matter around the galaxies of a selected type, averaged over all the galaxies in the sample. We can quantify this as an excess of the dark matter density above the average as a function of the radial separation r. This is described by the galaxy-dark matter cross-correlation function,

$$\xi_{\rm g,dm}(r) = \langle \delta_{\rm g}(\vec{x}) \delta^*_{\rm dm}(\vec{x}+\vec{r}) \rangle \, . \quad (1)$$

Here $\delta_{\rm g}$ and $\delta_{\rm dm}$ are the overdensities of galaxies and dark matter, respectively.

Observationally the quantity we are interested in is tangential shear γ_t, which describes elongation of images perpendicularly to the line connecting the image and the lens. This is related to the convergence $\kappa = \Sigma/\Sigma_{\rm crit}$, where Σ is the projected surface density in units of critical density,

$$\Sigma_{\rm crit}\gamma_t(R) \equiv \Delta\Sigma(R) = \bar{\Sigma}(R) - \Sigma(R). \quad (2)$$

Here R is the radial distance from the galaxy and $\bar{\Sigma}(R)$ is the mean surface density within R. $\Delta\Sigma(R)$ is the quantity that is observable, so all of our predictions will be compared to it. Critical surface density depends on the distances to the lens and source galaxies,

$$\Sigma_{\rm crit} = \frac{c^2}{4\pi G}\frac{D_S}{D_L D_{LS}}, \quad (3)$$

where D_L and D_S are the angular diameter distances to the lens and source, respectively, and D_{LS} is the angular diameter distance between the two. In the case of SDSS we know the redshift of the lens, so D_L is known, while D_S and D_{LS} can only be determined in an average sense. Since SDSS survey is so shallow, the redshift distribution of background galaxies is well determined from other deeper redshift surveys such as CNOC (Lilly et al. 1995). This means that there is little error associated with the redshift distribution of background population, which is not the case for deeper lensing surveys. While there is some uncertainty in the transformation from redshifts to distances this is generally a small effect given the low redshifts of background population ($z \sim 0.3 - 0.5$). Here we will ignore it, assuming distances using cosmological constant model with matter density $\Omega_m = 0.3$.

To relate the observations to theory we interpret the above expressions in an average sense by averaging over all the galaxies and their surrounding dark matter. In this case the surface density Σ is related to the galaxy-dark matter correlation function (Guzik & Seljak 2001)

$$\Sigma(R) = \int \bar{\rho}\xi_{\rm g,dm}[(R^2+\chi^2)^{1/2})d\chi, \quad (4)$$

where we dropped the unobservable constant term. Since we are interested in the small scales where galaxies do not evolve much we will express everything in proper coordinates. The low mean redshift of lens population ($\bar{z} \sim 0.1$) and the fact that most of the galactic halos have formed at higher redshift means that the redshift evolution effects will be small if expressed in proper coordinates and relative to the matter density today. We are implicitly assuming that most of the signal is arising near the galaxy, so we ignore the changes in the focusing strength along the line of sight.

2.2 Halo model

For a given correlation function $\xi_{\rm g,dm}$ we can use equations (2-4) to calculate $\Delta\Sigma$. In the halo model it is easier to calculate the power spectrum $P_{\rm g,dm}(k)$, which is just the Fourier transform of the correlation function. The halo model for power spectrum assumes the matter is in a form of isolated halos with a well defined mass M and halo profile $\rho(r, M)$. The latter is defined to be an average over all halos of a given mass and does not assume all halos have the same profile. The mass is determined by the total mass within the virial radius $r_{\rm vir}$, defined to be the radius where the mean density within it is $\delta_{\rm vir}$ times the critical density of the universe. Here we will use the value $\delta_{\rm vir} = 200$ relative to the critical density today. Often one uses the value defined by the spherical collapse model, which gives $\delta_{\rm vir} \sim 100$ for ΛCDM model with $\Omega_m = 0.3$. The latter gives about 15% higher

virial mass than the values presented here for a typical halo profile.

We model the halo density profile in the form

$$\rho(r) = \frac{\rho_s}{(r/r_s)^{-\alpha}(1+r/r_s)^{3+\alpha}}. \quad (5)$$

This model assumes that the profile shape is universal in units of scale radius r_s, while its characteristic density ρ_s at r_s or concentration $c = r_v/r_s$ may depend on the halo mass. The halo profile is assumed to scale as r^{-3} in the outer parts and as r^{α} in the inner parts, with the transition between the two at r_s. We fix the inner slope to $\alpha = -1$ (Navarro, Frenk, & White 1997), since SDSS g-g lensing is not sensitive to small scales given that the first bin is at $R = 75h^{-1}$kpc. For this profile the typical concentration on galactic scales is expected to be $c_{200} \sim 10$ (Bullock et al. 2001, Eke, Navarro, & Steinmetz 2001). We explore the sensitivity of g-g lensing to this parameter below.

The first contribution to the one-halo or Poisson term comes from the dark matter halos attached to the galaxy, where the galaxy is assumed to be at the halo center. If all the galaxies were of the same mass then this term would be just the Fourier transform of the dark matter profile itself. A generalization of this is to integrate over the luminosity distribution assuming a relation between the galaxy luminosity L and halo mass $M(L)$,

$$P^{\rm cg}_{\rm g,dm}(k) = \frac{1}{(2\pi)^3 n}\int \frac{dn}{dL} y[k, M(L)]dL, \quad (6)$$

where dn/dL is the known luminosity distribution of the lens sample and n is the total number of galaxies in the sample. The superscript cg stands for central galaxy. Here $y(k,M) = \tilde{\rho}(k,M)/M$, where $\tilde{\rho}(k,M)$ is the Fourier transform of the radial halo profile of dark matter

$$\tilde{\rho}(k,M) = \int 4\pi r^2 dr \rho(r,M)\frac{\sin(kr)}{kr}. \quad (7)$$

Note that unlike in previous work on halo model we do not require the profile to stop at the virial radius, so there can be more mass associated with the halo than the virial mass itself. This is only possible if we do not require the mass function defined below to integrate to unity, since some of the mass can be part of the extended halo structure beyond the virial radius. This is the case for the mass function by Jenkins et al. (2001) that we use here. Typically we extend the halo to 2-3 times the virial radius and we verified that the exact cutoff position makes very little difference in the final results. As discussed above we assume the dark matter profile for a given luminosity does not depend on whether a galaxy is in a larger halo or not. In the extreme case that the galaxies within larger halos do not have any mass attached to them at all the virial masses of field galaxies should be underestimated by the fraction of galaxies in groups and clusters. Most of these galaxies are in fact in the field, so this fraction and the corresponding correction is small.

Second contribution to the one-halo term comes from the dark matter around galaxies in groups and clusters, where the dark matter is not associated with the galaxy but with a larger halo. This term by definition includes only the galaxies that are not at the center of the halo they find themselves in, since such galaxies are already accounted for by the previous term. To obtain the g-g signal one must average over the mass distribution of halos and over the distribution of galaxies within these halos. Since the halos come in a variety of sizes we must first introduce the halo mass function dn/dM, describing the number density of halos as a function of mass. It can be written as

$$\frac{dn}{d\ln M} = \frac{\bar{\rho}}{M} f(\sigma)\frac{d\ln\sigma^{-1}}{d\ln M}, \quad (8)$$

where $\bar{\rho}$ is the mean matter density of the universe, M is the virial mass of the halo and $n(M)$ is the spatial number density of halos of a given mass M. We introduced a function $f(\sigma)$, which has a universal form independent of the power spectrum, matter density, normalization or redshift if written as a function of rms variance of linear density field σ. Jenkins et al. (2001) propose the following form (see also Sheth & Tormen 1999),

$$f(\sigma) = 0.315\exp[-|\ln\sigma^{-1} + 0.61|^{3.8}], \quad (9)$$

which they argue is universal if mass used is within the radius where overdensity is 200 of mean density (since we use a different definition of halo virial mass we must correct for the difference between the two). Note that this mass function does not account for all the mass density in the universe, so that some of the mass could be present in the outer parts of the halos.

We must still specify how the galaxies populate the halos of different mass. For any galaxy sample this can be parametrized as the mean number of galaxies as a function of halo mass $\langle N\rangle(M)$ (Jing, Mo, & Boerner 1998). Here we work with $\langle N\rangle(M)$ averaged over the luminosity distribution of the sample, which is dominated by the galaxies around $L_\star$ (see figure 1). We describe a model for $\langle N\rangle(M)$ below. The contribution from this term is

$$P^{\rm gc}_{\rm g,dm}(k) = \frac{1}{(2\pi)^3\bar{n}}\int f(\sigma)d\ln\sigma\langle N\rangle y(k,M)y_g(k,M), \quad (10)$$

where y_g is defined as the Fourier transform of the radial distribution of galaxies and the superscript gc stands for group and cluster contribution. We will assume $y_g = y$ in most of this paper, but we also explore the sensitivity to this assumption in the next section.

Finally, the halo-halo contribution to the power spectrum describes the correlations between the lens galaxy and neighbouring halos. Here we assume it follows the linear power spectrum, except that halos can be biased relative to it, with bias $b(\sigma)$ a function of rms variance σ. This assumption has been shown to give a good agreement with simulations of galaxy-dark matter correlations (Seljak 2000). Low mass halos are unbiased or mildly antibiased ($b \le 1$, Sheth, Mo, & Tormen 2001). The power spectrum of this term can be calculated using (Seljak 2000)

$$P^{hh}_{\rm g,dm}(k) = P_{\rm lin}(k)\left[\frac{\bar{\rho}}{\bar{n}}\int f(\sigma)d\ln\sigma\frac{\langle N\rangle}{M}b(\sigma)y_g^p[k,M(\sigma)]\right] \times \left[\int f(\sigma)d\ln\sigma b(\sigma)y[k,M(\sigma)]\right], \quad (11)$$

where $p = 0$ for the field component and $p = 1$ for the group/cluster component. Here we implicitly assumed that $\langle N\rangle(M)$ includes also the central galaxy component, which means it will have a strong peak at the halo mass corresponding to the $L_\star$ luminosity (figure 1). Since we will show that this term is negligible on the scales below $1h^{-1}$Mpc of

interest here the details of its modeling are not very important for our purpose.

The total power spectrum is simply the sum of all contributions. Once this is computed we Fourier transform it to obtain the correlation function and integrate it along the line of sight (equation 4) to obtain the projected surface density $\Sigma(R)$. Another integration (equation 2) is needed to obtain the mean surface density within R and the observed quantity $\Delta\Sigma(R)$. Since the redshift of lenses is low we do not include any redshift evolution effects.

The above model left several functions unspecified, most notably the halo mass-luminosity relation and the galaxy occupation number $\langle N\rangle(M)$. We assume that there is a one to one correspondence between the halo mass and luminosity of the galaxy, which we model as a power law

$$\frac{M}{M_\star} = \left(\frac{L}{L_\star}\right)^\beta, \tag{12}$$

where $M_\star$ is the mass associated with $L_\star$ galaxy. The slope β parametrizes the relation for a simple power law dependence. This is not the most general possibility and over a broad range of luminosity β is expected to vary, but since we are working over a narrow range of luminosities (a factor of 10 at best) this parametrization should not be too bad and in any case, the data do not yet allow for a more general parametrization. Note that bright red galaxies have been removed from the sample, since it is likely that they do not fall on the same mass-luminosity relation. Both $M_\star$ and β can be extracted from the data. We could also give some scatter to this relation, but in practice the scatter is dominated by the fact that we cannot choose very narrow luminosity bands for the analysis and so we will not pursue it further here. The distribution of halo masses has a width that depends on the luminosity distribution of the galaxies as shown in figure 1.

The second unspecified function is the galaxy occupation number $\langle N\rangle(M)$ for noncentral galaxies in groups and clusters. This is expected to grow with the halo mass for any galaxy population. Here we assume that the mean number of galaxies (of a given type) has a power law relation to the mass of the halo,

$$\langle N\rangle \propto M^\epsilon, \quad M > M_{\rm cutoff}. \tag{13}$$

We assume the power law relation is valid from some minimum halo mass $M_{\rm cutoff}$, which should be at least a few times above the typical halo mass for a given luminosity sample, since by definition it is assumed these galaxies are not at the halo centers, where presumably another bright galaxy resides. We explore the sensitivity to the low mass cutoff $M_{\rm cutoff}$ and ϵ below. We normalize the group/cluster contribution in terms of a fraction of galaxies α that reside in these larger halos.

In figure 2 we show $\langle N\rangle/M$ versus M as calculated from semi-analytic simulations (Kauffmann et al. 1999) for two narrow intervals in luminosity, a brighter one around $L_\star$ and a fainter one magnitude below it. One can see that in both cases the distribution is well modeled as a sum of a narrowly peaked distribution for the central galaxies and a linear power law component $\langle N\rangle \propto M$ for the noncentral galaxies in groups and clusters. In our model we would predict first contribution to be narrow because we have chosen a narrow bin in luminosity, which is strongly correlated with the halo mass for central galaxies. This is clearly seen to be the case in figure 2. Second contribution is a power law because more massive halos also contain more subhalos of a given mass, which host noncentral galaxies. It is the latter contribution that enters in our model for $\langle N\rangle/M$ in equation 6, while the first component is included by the galaxy luminosity function. Our model therefore qualitatively reproduces the main features of SAMs, but by characterizing the main ingredients with a few free parameters it allows us to be more general than any specific model.

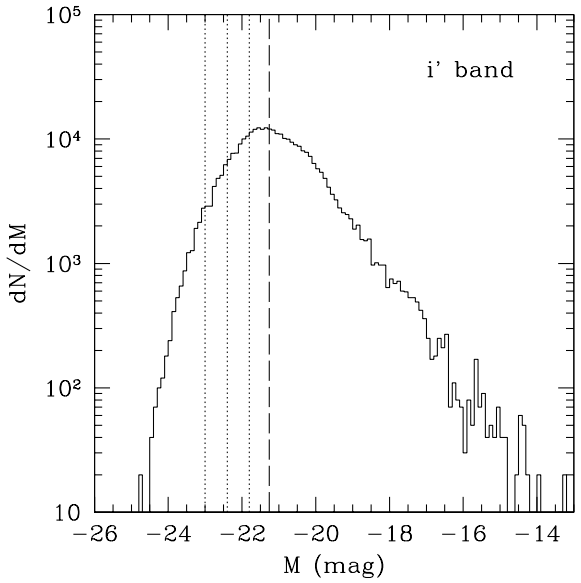

Figure 1. Magnitude distribution of the SDSS sample in i' band (in units with $h = 1$) for the whole sample and the 4 luminosity subsamples separated by dotted lines. Also indicated is the $L_\star$ magnitude (Blanton et al. 2001) as a vertical dashed line, which roughly corresponds to the mean luminosity of the whole sample ($\langle L\rangle \sim L_\star = 2.05\times10^{10}h^{-2}L_\odot$). Note that even though the mean luminosity is close to $L_\star$ most of the lensing signal comes from the massive galaxies above $L_\star$, which explains the choice of luminosity subsamples.

It is interesting to compare the fraction α of galaxies in groups/clusters for the two cases from figure 2. This is 20% for the bright sample and 25% for the faint sample. This parameter can therefore vary as a function of luminosity and is expected to decrease with L. This means that the group/cluster contamination is less important for bright galaxies, where it becomes more difficult to determine it observationally because of the small number statistics. We will use this fact in the modeling below.

3 DEPENDENCE OF G-G LENSING ON THE HALO MODEL PARAMETERS

3.1 Halo mass and concentration

We have introduced several free parameters in the model above and in this section we explore the dependence of the measured signal on them. The main parameter is the virial halo mass $M_\star$ of a typical $L_\star$ galaxy. The resulting g-g lens-

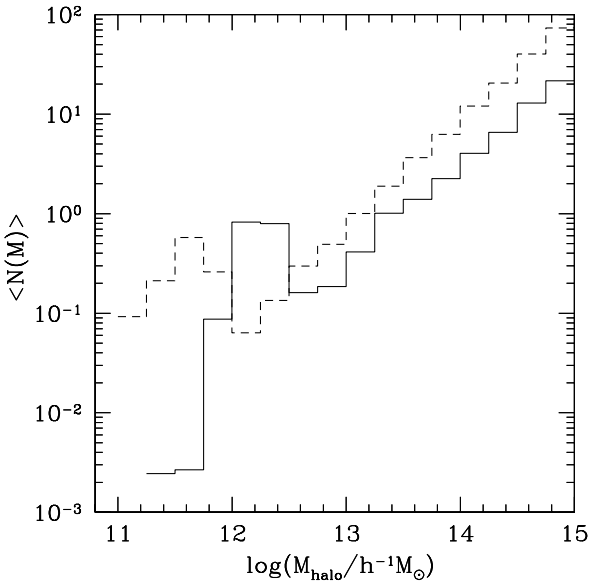

Figure 2. $N(M)$ calculated from SAMs using GIF simulations (Kauffmann et al. 1999) using two narrow luminosity samples, $-20.5 < I < -20$ (dashed) and $-22 < I < -21$ (solid). Both the central galaxy component peaking at low halo masses and non-central group/cluster component are included here. The latter has $N(M)$ approximately proportional to M, ie $\epsilon = 1$.

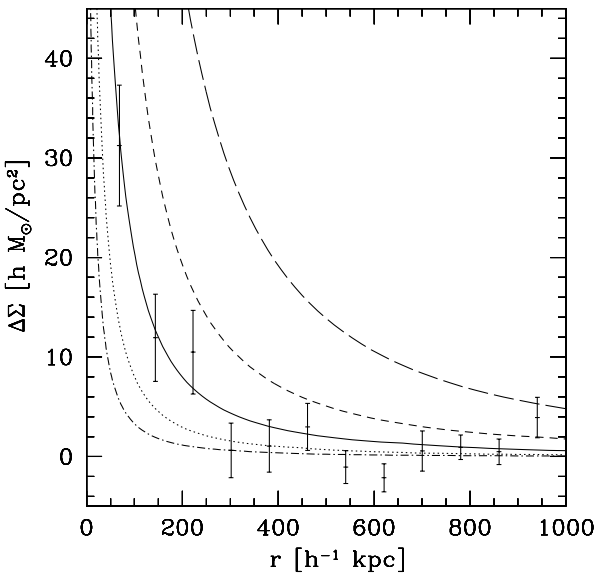

Figure 3. Signal for a NFW halo profile with $c = 10$ of varying mass. From bottom to top $M = 10^{11}, 3 \times 10^{11}, 10^{12}, 3 \times 10^{12}, 10^{13} h^{-1} M_\odot$. Also shown are the observational data for the low density sample.

ing signal for halos of masses between $10^{11} - 10^{13} h^{-1} M_\odot$ is shown in figure 3. For reference we also show the SDSS data using the low density subsample, described in more detail below. Only the one-halo term is shown and we used NFW profile with $c = 10$ and a δ-function in the halo mass distribution. What is shown is therefore a simple projection of NFW profile, which has a well known analytic form for $\Sigma(R)$ (Bartelmann & Schneider 2001). The signal at a given scale is rapidly increasing with the mass of the halo, indicating that SDSS g-g lensing is a very sensitive probe of the virial mass of the halo. Masses around $10^{12} h^{-1} M_\odot$ seem to be required to explain the field sample.

The dependence on the concentration parameter c is shown in figure 4. We keep the virial mass of the halo constant, so the signal at large radii is similar for all the models. At smaller radii the profiles start to differ and the more concentrated halos give a larger signal than the less concentrated ones. Doubling the concentration index c changes the signal by 20-30% in the inner most bin at $75 h^{-1}$kpc and less than that at larger radii. We will see below that since some contribution to the mass determination comes from the inner most bin there is some degeneracy between c and M, such that larger values for c give lower values for M. However, this degeneracy is not complete and too steep profiles can be ruled out regardless of the halo mass.

Since we cannot choose an infinitely narrow distribution in luminosity and have a high signal to noise a δ-function in the halo mass distribution is not very realistic. Instead one must integrate over the halo mass distribution to obtain the average profile. While the mean signal will correspond to the mean halo mass, the shape of the signal may be more affected, possibly complicating the determination

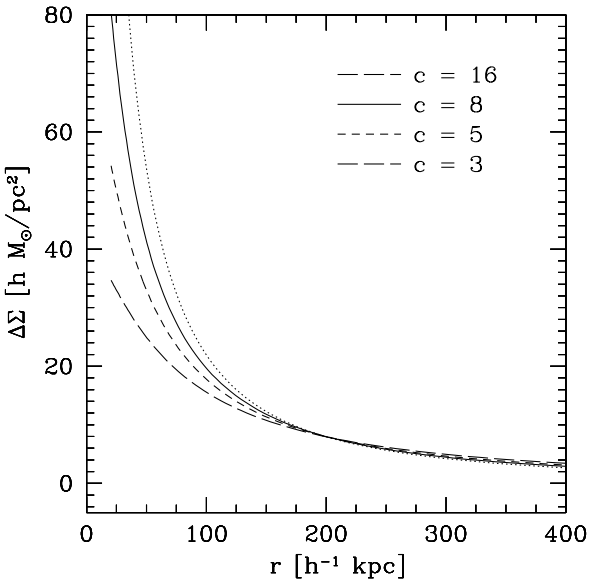

Figure 4. Signal for a halo with NFW profile of fixed mass varying concentration c from 3 to 16.

of the concentration parameter. To investigate this possibility we compute the signal for the luminosity distribution in figure 1, assuming halo mass is proportional to luminosity and comparing it to a single NFW profile corresponding to the mean mass of the sample. The result is shown in figure 5. The two profiles are very similar, indicating that even for realistic luminosity distributions the shape of the halo can be reliably determined from the data if all the galaxies are

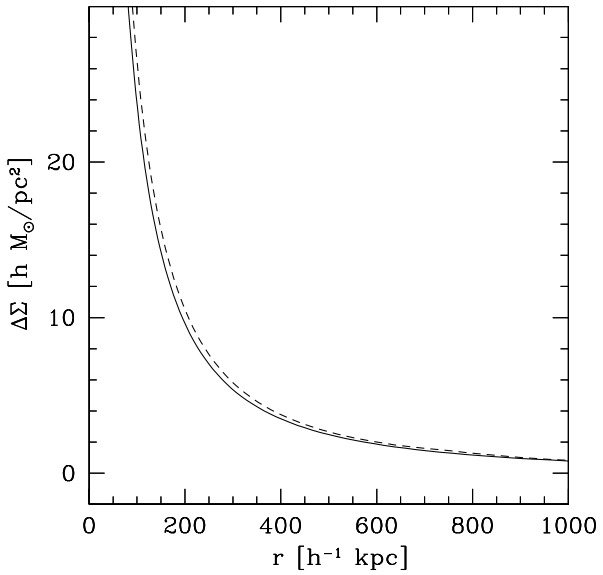

Figure 5. Comparison between a single NFW profile for $M_\star$ (solid) and an average profile using the realistic luminosity distribution and assuming luminosity is proportional to mass (dashed).

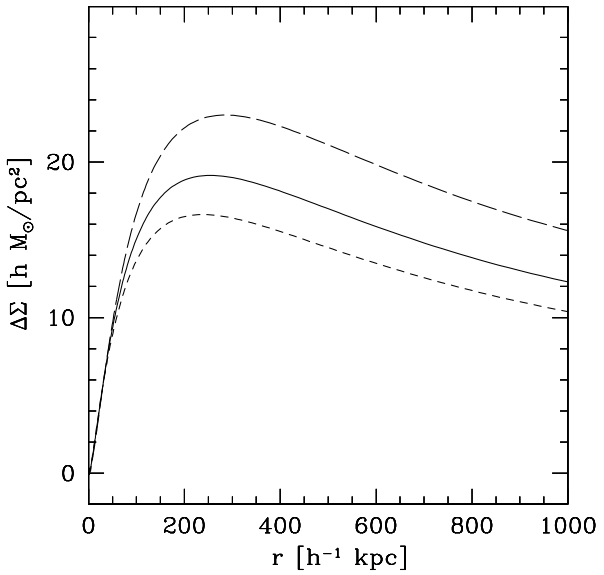

Figure 6. Group and cluster contribution to g-g lensing as a function of lower mass cutoff $M_{\rm cutoff}$. Results shown here are for $M_{\rm cutoff}$ of $10^{12}h^{-1}M_\odot$ (bottom curve), $3\times10^{12}h^{-1}M_\odot$ (middle curve) and $10^{13}h^{-1}M_\odot$ (top curve). We use $c=7$ for galaxy and dark matter halos.

at the halo centers. These results show that if the galaxies are in the field then g-g lensing is a very robust probe of the halo virial mass and its profile. The field assumption should be valid for the low density sample discussed in more detail below. For the whole sample one must introduce also the contribution from groups and clusters, which is discussed next.

3.2 Group and cluster contribution

The group and cluster contribution to lensing is shown in figure 6 for $\epsilon = 1$. Here it is assumed all the galaxies are in groups and clusters ($\alpha = 1$). It is evident that this contribution is significantly different from the central galaxy contribution. At small radii the group/cluster contribution is negligible, since by definition these galaxies are not at the halo center (the individual subhalo contribution from these noncentral galaxies is already included in the previous term), the cluster component itself is very smooth and the galaxies are assumed to be distributed radially like dark matter and do not have a strong central peak. We remind the reader that for a uniform density the shear signal goes to zero by equation 2. The group/cluster contribution peaks around $200h^{-1}$kpc and then gradually decreases with radius, such that even at $1h^{-1}$Mpc it is still 60% of the peak value. One can see that varying the low mass cutoff $M_{\rm cutoff}$ has some effect on the amplitude of the signal. For lower mass cutoffs one finds a lower average signal, because there are proportionally more galaxies in less massive halos. On the other hand, the radial dependence of this contribution is less affected. Since the radial dependence of this contribution is very different from the central galaxy contribution (figure 3) the two contributions can be robustly separated in the data even if the actual value of α has some uncertainty related to the low mass cutoff. Based on the results in figure 2 we choose $M_{\rm cutoff}$ to be 3 times the halo mass corresponding to the luminosity of the sample. For $L_\star$ galaxies this is around $2\times10^{12}h^{-1}M_\odot$. This cutoff is increased when we analyze brighter luminosity subsamples.

In addition to the group low mass cutoff we also explored the sensitivity of this component to the slope ϵ of the galaxy occupation number (equation 13) and to the radial galaxy distribution y_g (equation 6). The results are shown in figure 7. Higher ϵ gives more weight to more massive clusters and has a higher signal than a lower ϵ. Similarly, more concentrated galaxy distribution enhances the signal since now more galaxies are closer to the cluster center where the halo density is higher. Most observations and simulations predict that galaxy distribution does not deviate significantly from the dark matter, which has a mean concentration of around $c = 5-10$ for groups and clusters, depending on the low mass cutoff. Here we compare the cases with $c = 3, 7, 10$ for the galaxy while using $c = 7$ for the dark matter. In all cases the overall amplitude changes somewhat depending on the parameters, while the qualitative shape of the curve remains similar, peaking around $200h^{-1}$kpc and then decreasing with radius. This is distinguishable from the central galaxy component regardless of the specific choice of the parameters. In the following we assume $\epsilon = 1$ and $y_g = y$ with $c = 7$.

To combine the central galaxy and group and cluster contributions we must assume parameter α, which is the fraction of galaxies in groups and clusters. Variation in this parameter is shown in figure 8. If the fraction α is small the signal on large scales is also small, whereas in the opposite case the large scale and small scale signals are comparable. Also shown are the data from the whole SDSS sample, which show a relatively flat signal between 300-

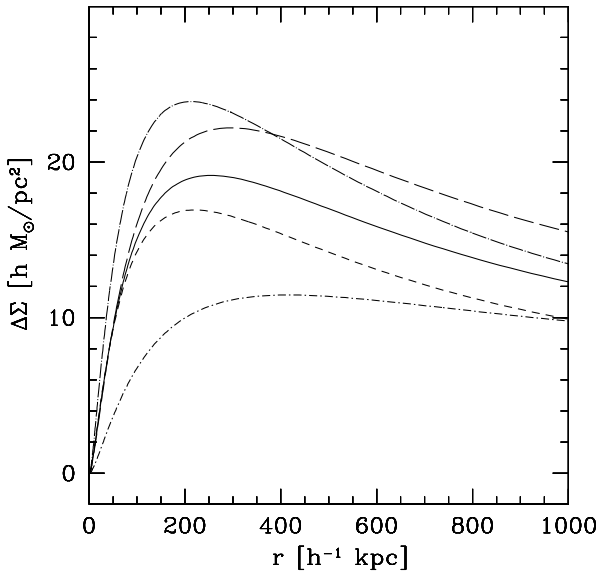

Figure 7. Group and cluster contribution to g-g lensing as a function of ϵ=0.8, 1.0, 1.2 (short dashed, solid, long dashed, respectively) and using $c = 7$ for galaxy and dark matter. Also shown is variation of radial galaxy distribution parametrized with concentration $c = 3$ (dot-short dashed) and $c = 10$ (dot-long dashed) for $\epsilon = 1$.

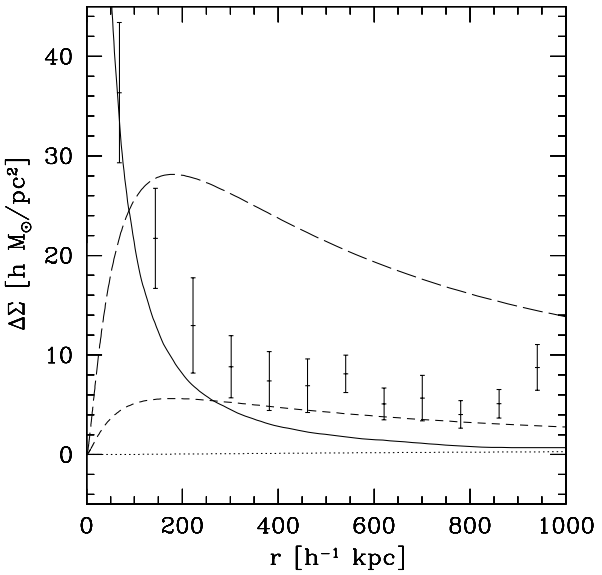

Figure 8. Central galaxy contribution for $M_\star = 10^{12}h^{-1}M_\odot$ (solid), group/cluster contribution with $\alpha = 0.2$ (short dashed) and $\alpha = 1$ (long dashed) and halo-halo contribution to g-g lensing (dotted). Also shown is the SDSS data for the whole sample.

$1000h^{-1}$kpc. This cannot be explained by the central galaxy contribution alone, which drops below the observed points at $R > 200h^{-1}$kpc. It also cannot be explained by all the galaxies being in groups and clusters, which would have an excess of signal at large radii. A contribution from noncentral galaxies in groups and clusters with $\alpha = 0.2$ together with the central galaxy contribution provides a good description of the data.

The contribution from the correlations between the galaxies and the neighbouring halos (halo-halo term) is also shown in figure 8. This contribution is very small and cannot explain the strength of the signal on scales around 300-$1000h^{-1}$kpc. Instead the group and cluster contribution is required to explain the signal on these scales. Note that this does not mean that the correlations between the galaxies are not important, since the galaxies residing in groups and clusters are also correlated among themselves. It does however mean that the correlations between the galaxies in isolated halos are small and are instead dominated by the galaxies that reside in groups and clusters, whose contribution to g-g lensing is included in group and cluster term discussed above. The main difference between the two terms is that for the latter most of the mass in large halos is not associated with the halos of individual galaxies within them, which account for only about 5-10% of the mass, but with a diffuse component of groups or clusters. In this respect our analysis differs from the previous analysis of this data (McKay et al. 2001), where only the mass associated with the visible galaxies was accounted for in the correlation analysis.

4 APPLICATION TO THE SDSS DATA

In this section we apply the formalism developed in previous sections to the SDSS data. We begin first by analyzing the luminosity dependence of g-g lensing, which provides us with a parametrization of the mass luminosity relation and with a typical mass $M_\star$ of an $L_\star$ galaxy. We proceed by analyzing the full sample as well as high and low density versions of it, which provide an alternative estimate of $M_\star$ and the fraction α of group/cluster galaxies in the sample, as well as an estimate of mass loss in dense enviroments. Finally, we address the morphological dependence of the signal, which helps to explain some of the trends in mass-luminosity dependence.

4.1 Luminosity dependence

In this subsection we model the luminosity dependence of the signal using the g-g lensing as a function of galaxy luminosity in all 5 SDSS colors. The lenses have been divided into 4 luminosity bins, with the mean luminosity varying between $0.6L_\star$ to $7L_\star$ (see figure 1). In all cases the quantity we analyze is $\Delta\Sigma(R)$, averaged in equally spaced radial bins. We assume that the errors between bins are independent. This is a good approximation at small separations, where a given background galaxy contributes typically only to one lens galaxy (average separation between the lens galaxies is around $300h^{-1}$kpc). At larger separations this assumption breaks down, but since we will be mostly focusing on the inner regions this will not be a significant factor for the results of the fits (although it may affect the goodness of fit, see below).

The data divided in luminosity bins do not have sufficient statistical signal to allow accurate determination of group/cluster fraction in each bin separately. Since this frac-

tion is expected to decrease with luminosity (figure 2) and it is already low in the lowest luminosity bin we make the fits using two different assumptions. In the first we assume $\alpha = 0$ for all but the lowest luminosity bin. In the second we assume α from the lowest luminosity bin also applies to the higher luminosity bins and we use luminosity dependent $M_{\rm cutoff}$ roughly 3 times above the mass corresponding to that luminosity. Since α is expected to decrease with luminosity the answers we get from the two models should bracket the real values. We do not fit for the mean mass in each bin separately, but use the power law relaton between luminosity and mass to fit for $M_\star$ and β.

The results from the fits for both cases are given in table 1 and shown in figures 11 and 12. The contour plots for $M_\star$ and β are shown in figures 9, 10 for all bands. As one can see from table 1 except for the bluest band u' the relation between luminosity and mass is well established, as already shown by the SDSS team (McKay et al. 2001). The origin for lack of correlation in u' is the morphology dependence of the signal, as discussed in more detail below. In red bands the best fitted value for β is significantly above unity, indicating that the virial mass to light ratio is increasing with the halo mass (or luminosity). If light is a good tracer of stellar mass (as expected in the reddest bands) this indicates that the star formation efficiency is decreasing with luminosity. For example, in i' the fitted values are $M_\star = (6 \pm 2) \times 10^{11} h^{-1} M_\odot$, $\alpha = 0.2 \pm 0.05$ and $\beta = 1.51 \pm 0.15$, so that the value $\beta = 1$ is more than 3-σ away from the best fitted value. This gives $M_{200}/L \sim 30 h M_\odot/L_\odot$ at $L_\star$, which is the lowest luminosity that still has a detectable signal. This increases to $M_{200}/L \sim 80 h M_\odot/L_\odot$ at $7L_\star$ corresponding to the brightest luminosity bin. If instead M_{100} is used as the virial mass then these values should be increased by an additional 15%. These results however still hide significant variations between morphological types, as discussed below. Note that there is a strong correlation between $M_\star$ and β. This is because even though $L_\star$ is close to the mean luminosity of the sample, the luminosity distribution is broad and most of the signal comes from the brighter end of the luminosity distribution. An increase in β gives more mass to brighter galaxies, which allows for a lower $M_\star$ to fit the data.

In figure 11 the best fitted model is compared to the data in i' band for the case where $\alpha = 0$ except in the lowest luminosity bin. The model provides a reasonable fit to the data. The reduced χ^2 is around 2.4, indicating that the fit is not perfect, although there is no obvious systematic deviation that would indicate a clear shortfall of the model, suggesting instead that the observational error bars may be somewhat underestimated. One explanation for this is neglection of correlations between the bins, although this should only be important at large radii. Figure 13 shows the best fitted model assuming $\beta = 1$. For this case we find $M_\star = 1.5 \times 10^{12} h^{-1} M_\odot$ in i', but the fit is less good now.

For the case with the same value of α for all 4 bins we typically find $M_\star$ is about 15% lower as shown in figure 10 and in table 1, because part of the signal in the high luminosity bins is now accounted for by the group/cluster contribution. The slope β is reduced as well. The reduced χ^2 reduces to 2, so this procedure does somewhat better in describing the data, as shown in figure 12. The value for β does not change significantly (figure 10).

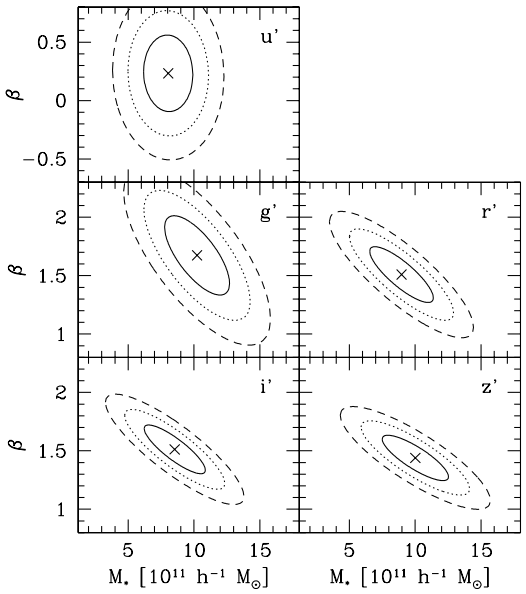

Figure 9. 68%, 95% and 99% contour plots for β and $M_\star$ as a function of SDSS color for the case $\alpha = 0$ in all but the lowest luminosity bin. The results are consistent with $M_\star \sim 6 - 8 \times 10^{11} h^{-1} M_\odot$ and $M/L \propto L^{1/2}$ except in u' where no clear correlation between light and mass is detected.

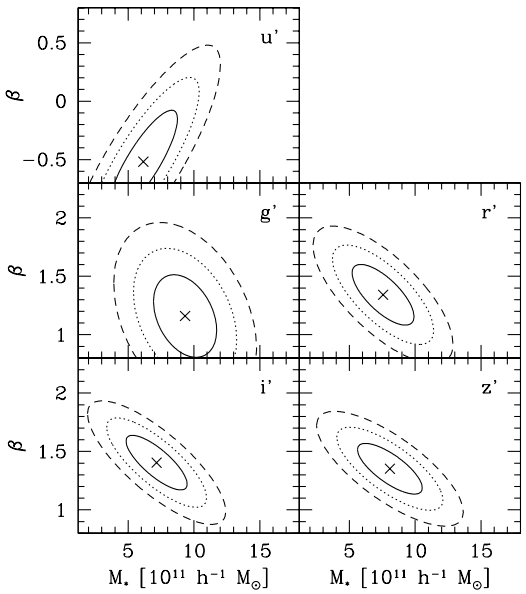

Figure 10. Same as 9 but with equal α in all luminosity bins.

4.2 Density selection and the fraction of group/cluster galaxies

In previous subsection we analyzed the luminosity dependent data to obtain the relation between the mass and luminosity around $L_\star$ galaxies. In this section we combine the

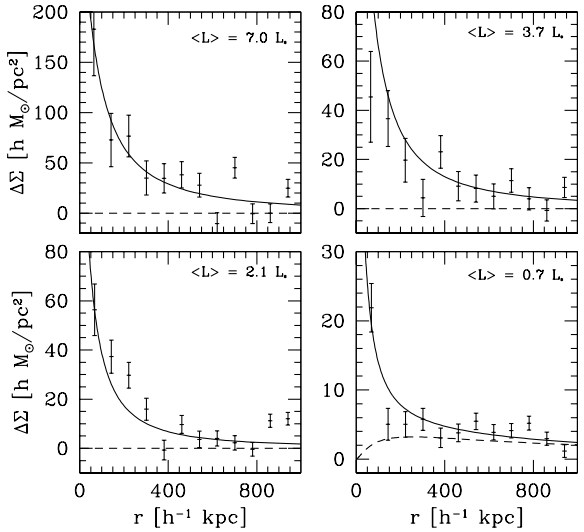

Figure 11. Dependence of the g-g signal on luminosity using the 4 subsamples in i' (figure 1) together with the best fitted model (solid). Dashed shows just the group and cluster contribution. We assume $\alpha = 0$ except for the lowest luminosity bin.

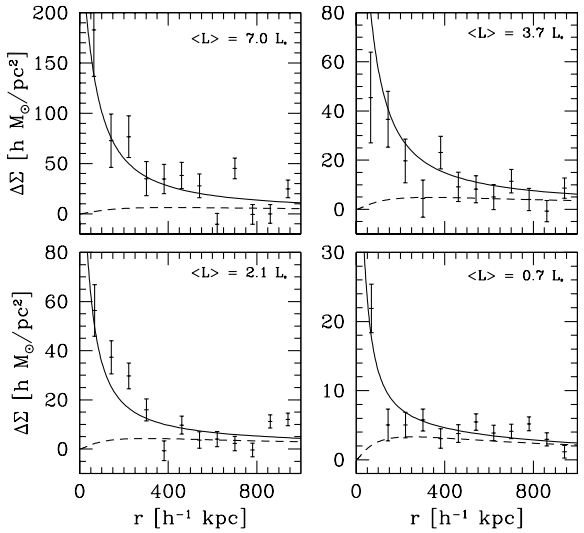

Figure 12. Same as figure 11 but with same α in all luminosity bins.

luminosity data into a complete sample of galaxies ⋆. This

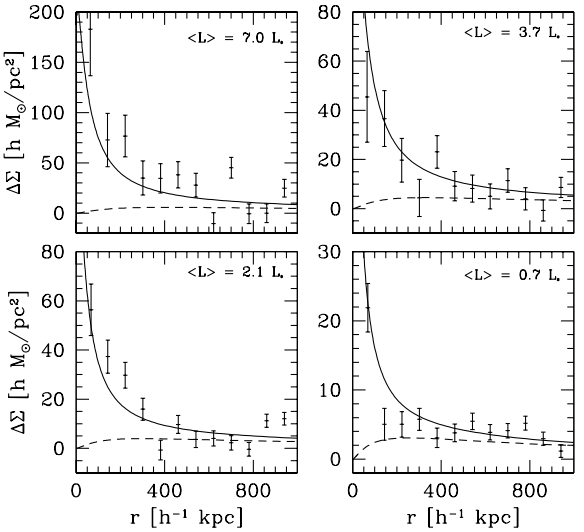

Figure 13. Same as figure 12 but with $\beta = 1$.

allows us to determine more accurately the fraction of galaxies in groups and clusters, which could not be modeled for each luminosity bin separately. Using β from the previous subsection and the actual luminosity distribution (figure 1) we fit for $M_\star$ and α. In i' we find $M_\star = (6\pm1)\times10^{11}h^{-1}M_\odot$ and $\alpha = 0.19 \pm 0.03$. These values are consistent with the values obtained in previous subsection for the case with α independent of luminosity. The resulting fits are shown in figure 14, where we see that the model provides a good description of the data (reduced $\chi^2 \sim 1$). It is clear that both the central galaxy and the group/cluster components are needed to explain the data.

To further test the obtained values we use the data split into high and low density enviroments (McKay et al. 2001). The separation is done using Voronoi tesselation, which assigns a weight to each galaxy according to the local density of galaxies. The galaxies are then rank ordered and divided into two equal samples. Both samples have roughly equal average luminosity, so under the assumption that luminosity scales with mass independent of enviroment the estimated $M_\star$ should be approximately equal. The resulting fits are shown in figure 15. For the low density sample the best fit gives slightly negative $\alpha = -0.07$, showing that the low density sample is consistent with the galaxies being only in the field. The best fitted mass in this case is $M_\star = (6-7)\times10^{11}h^{-1}M_\odot$ depending on the passband. If we assume $\alpha = 0$ then we find $M_\star = (4.5\pm1.5)\times10^{11}h^{-1}M_\odot$ for the low density sample in i'. For the high density sample the values are $M_\star = (5-8)\times10^{11}h^{-1}M_\odot$ and $\alpha = 0.45 \pm 0.04$. Assuming $\alpha = 0$ for low density sample one would expect

⋆ Note that averaging the luminosity bins does not give the same result as the average given in McKay et al. (2001). The reason for the difference is the clustering correction applied to the data. Since some fraction of background galaxies is correlated with the lens they do not contribute to the lensing, so one must correct upwards the measured signal. This correction increases with the luminosity of the lens galaxy and the proper procedure is to apply the correction to the luminosity dependent sample and then average the luminosity bins. Future data with better photometric redshift information for the background galaxies may allow one to eliminate this procedure by selecting only background galaxies that are far from the lens.

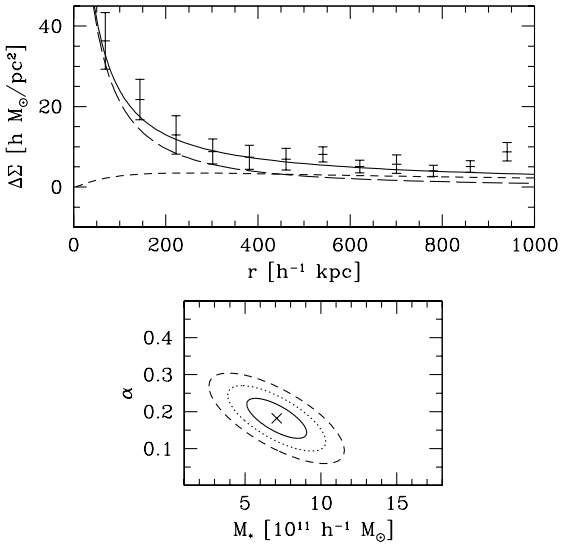

Figure 14. Top: best fitted model (solid) to the complete sample with parameter values given in the text. Also shown are central galaxy contribution (long dashed) and group/cluster contribution (short dashed). We do not show the clustering (halo-halo) contribution, which is negligible. Bottom: contour plot of α and $M_\star$. We used luminosity distribution in i' for this plot.

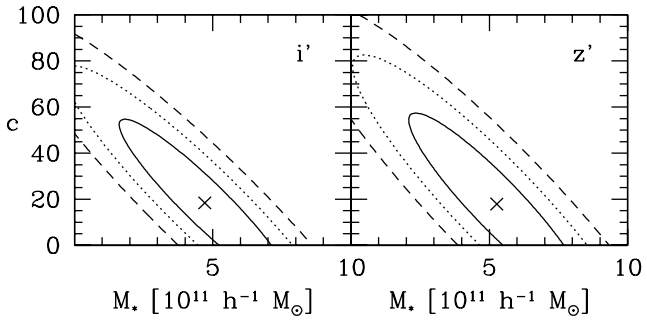

Figure 16. Contour plots in $c - M_\star$ plane for i' and z'. While the two parameters cannot be determined separately there is a weak dependence of $M_\star$ on c.

$\alpha \sim 2 \times 0.2 = 0.4$ for the high density sample using $\alpha \sim 0.2$ obtained from the complete sample. The actual value is consistent with this, giving another confirmation that our model contains all the main ingredients needed to explain g-g lensing. All the reduced χ^2 values are around 1, so the model fully explains the data.

We can test the assumption that for a given luminosity the halo mass and its profile does not depend on the enviroment by comparing the $M_\star$ between high and low density samples. If the galaxies inside larger halos do not keep any dark matter one should see a reduction in the high density sample at small radii, since for $1-\alpha = 0.6$ of all the galaxies there would be no individual halo attached to them. Such a model would give fitted $M_\star$ in the high density sample about 60% of that in the low density sample. In fact we find that the best fitted value for $M_\star$ are comparable, which argues against this assumption. While the errors are still large and the current data does now allow us to test this hypothesis in more detail we conclude that there is no evidence for a significant halo stripping or different star formation efficiency for galaxies within larger halos. This is consistent with the expectations from the noninteracting cold dark matter models (Ghigna et al. 2000), but may not be with self-interacting dark matter models which predict significant mass loss in subhalos (Spergel & Steinhardt 2000).

Since we have a signal as a function of radius we should be able in principle to place limits on the concentration parameter c independent of the halo mass. In practice broad luminosity distribution and significant clustering correction prevents us from doing so. We have tried to do a formal fit to $M_\star$ and c simultaneously and the resulting contour plots show a strong degeneracy between the two parameters (figure 16). Given that we cannot determine c independently we must asses its influence on $M_\star$. As seen in figure 16 there is some weak anti-correlation of $M_\star$ with c. This arises because higher c increases the signal in the first bin, which has a significant contribution to the overall fit. This correlation can be parametrized as $M_\star \propto c^{-0.15}$ and since c is expected to be in the range between 8 and 15 this uncertainty affects $M_\star$ by 10% at most and so does not dominate the error budget.

4.3 Morphology dependence

So far we have assumed that morphology of the lens galaxy does not affect the relation between luminosity and mass, so that we do not have to worry about their differences in a sample which mixes early and late types. This is a reasonable assumption in the red/infrared bands where light is supposed to be a reliable measure of the total stellar mass, assuming the morphology of a galaxy (which is believed to be related to the merging history) is not correlated with the amount of gas in a halo that cools to form stars. Observationally this was suggested by the SDSS team (McKay et al. 2001), showing that mass to light ratios at a fixed radius in the reddest bands were very similar. This analysis did not account for the contribution from groups and clusters and for observed mass-luminosity scaling. Here we assume mass luminosity relation based on β values in table 1. We use the sample split into late and early types that has about equal number of galaxies for the two types. The morphological classification is based on the color information and light concentration index and the early type sample is dominated by ellipticals, but also includes S0 and Sa galaxies, while the late type sample is dominated by Sb/Sc's (see Strateva et al. 2001 for a thorough discussion of the relation to the Hubble sequence). Figure 17 shows the fraction of the two types as a function of luminosity for the 4 bins used here. It is clear that at the bright end in r', i' and z', the sample is dominated by the early types, while in u' it is just the opposite. In g' the fraction is roughly independent of luminosity. Note that the bright end is where most of the g-g lensing signal is.

We fit for $M_\star$ and α in the two subsamples. The results are given in table 2 for all 5 colors. We do not apply

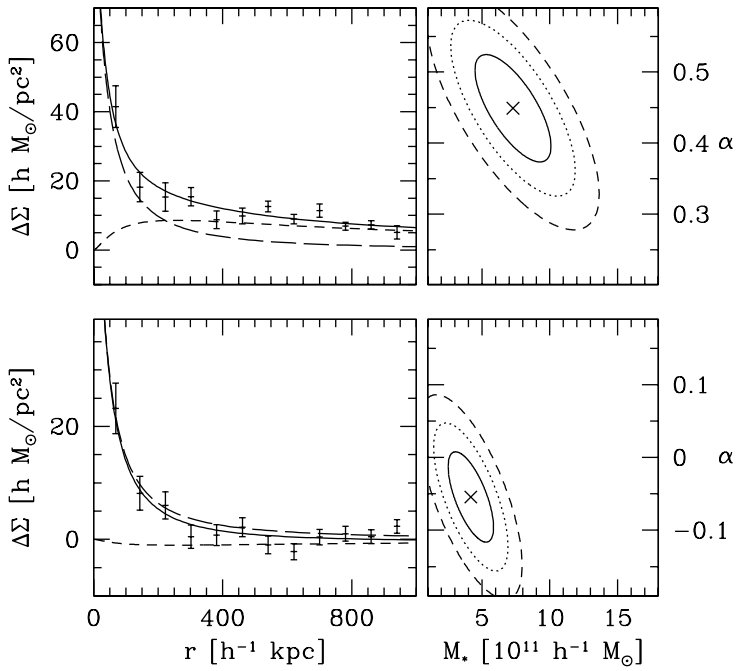

Figure 15. Top: best fitted model to the high density sample together with the contour plot in $M_\star - \beta$ plane for luminosity distribution in i'. Bottom: same for the low density sample.

any internal extinction correction which should be significant for the late type sample in the blue bands, so for those the intrinsic luminosities could be even brighter. In addition, while Petrosian magnitudes used by the SDSS should account for most of the light from the late types with exponential profiles they may underestimate the light from the early types with de Vaucouleurs profile by up to 20%. Figure 18 shows the best fitted model together with the data. We find $\alpha \sim 0.07 \pm 0.04$ for the late type sample, showing that most of the late type galaxies are in the field. For the early type galaxies we find $\alpha \sim 0.28 \pm 0.06$, so a significantly larger fraction of these is in groups/clusters. This is another evidence of morphology-density relation, although in this case we are not probing the relation as a function galaxy density (Dressler 1980), but rather the fraction of galaxies around $L_\star$ that are in groups of a broad range in mass around $10^{13} M_\odot$. Groups of such low mass are very difficult to study observationally and our approach is one of a few ways to study the galaxy membership in these halos. The errors quoted above are only statistical and the parameter α depends also on the assumed values for ϵ, $M_{\rm cutoff}$ and y_g as discussed in previous section. We estimate the systematic error on α should be of order 30%.

The values for $M_\star$ differ significantly between early and late types in all bands. The difference is almost a factor of 10 in u', 6 in g', dropping to a factor of 2.5 in r' and 2 in i' and z'. This differs somewhat from the conclusions in McKay et al. (2001), where it was found that M/L for the two types becomes equal in z'. The main reason for the difference is that we assume $M \propto L^\beta$ with β values from table 1 and that we apply luminosity dependent clustering correction to the data, which boosts the brighter early type sample more than the fainter late type sample. However, the error on $M_\star$ for the late types is large, since the signal is rather weak, and in i' and z' the data are still consistent with the assumption of equal M/L ratios for the two types. In addition, Petrosian magnitudes may miss up to 20% of light for early type profiles and much less than that for late types, so this may bring the mass to light ratios closer by this amount. Theoretically one would expect M/L to be quite similar if i' and z' luminosity is a reliable tracer of stellar mass and if star formation efficiency is independent of morphology. The color comparisons indicate that the difference in luminosity between early and late types is only 20-30% from i' to K band (which should be closest to tracing stellar mass). We discuss the validity of these assumptions further below.

Given that the M/L differs significantly between early and late types and that their relative contribution changes with luminosity we must revisit the mass-luminosity scaling of previous subsection. One possibility is to use g', where the two populations are in equal ratios across all luminosity bins. Since at a given luminosity late types are much less massive the dominant contribution comes from the early types, so the deduced $\beta = 1.3 - 1.7$ is the correct scaling for early types regardless of β for late types. In i' and z' the early types dominate at the brightest end and contribute only 40% to the faintest bin, so here a morphological dependence of M/L could induce a change in β. On the other hand, in these bands the late types are only a factor of 2 less massive for a given luminosity. This gives β for early types about

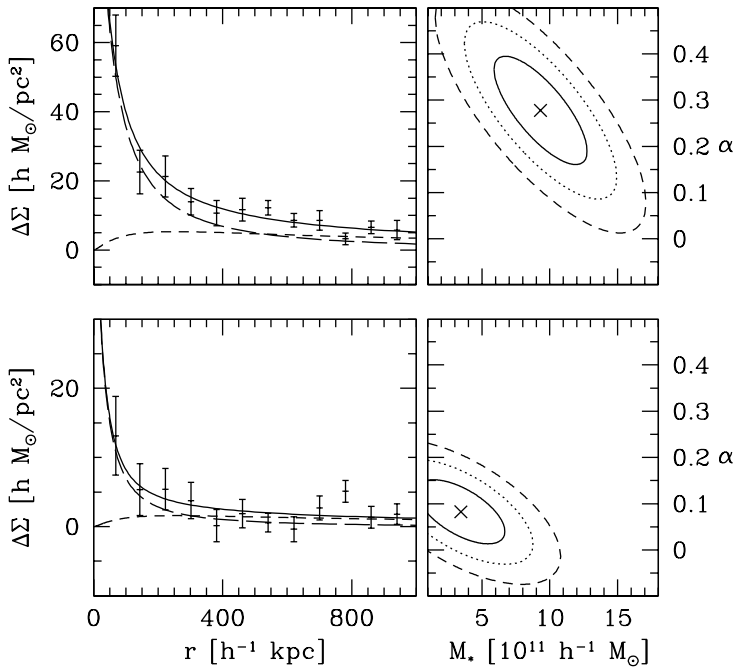

Figure 18. Top: best fitted model to the early type sample together with the contour plot in $M_\star - \alpha$ plane for luminosity distribution in i'. Bottom: same for the late type sample.

0.15 lower than the value found for the overall population. Similar values are found also in r' and z'. We conclude that β for early types is in the range 1.4 ± 0.2 in the red bands.

Variation of morphology with luminosity has a larger effect on the correlation between luminosity and mass in u'. Here late types dominate at the bright end and early types at the faint end, so the massive galaxies are actually on average fainter than the less massive ones. If we use $\beta = 1.4$ for early types together with the scaling of early type fraction with luminosity (figure 17) we obtain $\beta \sim 0.5$, in agreement with the fitted value in this band. Lack of correlation in this band is therefore not necessarily a consequence of u' light being uncorrelated with mass, but rather of a changing morphological fraction with luminosity coupled to a large difference in M/L at a given L in that band.

The current data sample does not allow for a determination of mass luminosity relation for late types. We have assumed the same value of β for both types here, but it could well be that β is lower for the less luminous and less massive late type sample, as suggested by the semi-analytic models of galaxy formation (Kauffmann et al. 1999, Benson et al. 2000). If we use $\beta = 1$ for the late type the best fitted $M_\star$ does not change much, so the difference in M/L between early and late type sample cannot be explained by this effect.

The errors in tables 1, 2 are assumed to be gaussian in $M_\star$, α and β. For $M_\star$ we show the comparison in figure 19, where the log-likelihood is plotted against the gaussian approximation for early and late type galaxies. We show both the case assuming a constant α (where the rms error is given by the inverse of corresponding diagonal term in the curvature matrix) and marginalized over α (where the rms error is given by the corresponding diagonal term in the inverse of curvature matrix). In all cases the gaussian approximation gives a good description of the true likelihood at least out to 2-sigma level. This is a consequence of the fact that the signal scales almost linearly with the virial mass $M_\star$ (figure 3).

Since for early types the group and cluster contribution is significant the values of $M_\star$ depend somewhat on the assumed radial distribution of galaxies and dark matter, as well as on the halo occupation statistics. We find that if the group and cluster profile is shallower then fitted values do not change much, while if they are more concentrated then part of the signal at smaller radii can be attributed to group/cluster contribution and this lowers $M_\star$. For example, assuming $c = 10$ both for group/cluster dark matter and for radial galaxy distribution results in a 25% reduction of $M_\star$ for early types, while the corresponding value for late types changes significantly less. This is probably an upper limit, since $c = 10$ is a more appropriate value for galaxy sized halos rather than groups and clusters, but one should nevertheless keep in mind this as an additional source of systematic error on $M_\star$.

5 DISCUSSION

This paper establishes a quantitative framework on how to analyze g-g lensing data and applies it to the SDSS sample of 35,000 galaxies with known redshifts and luminosi-

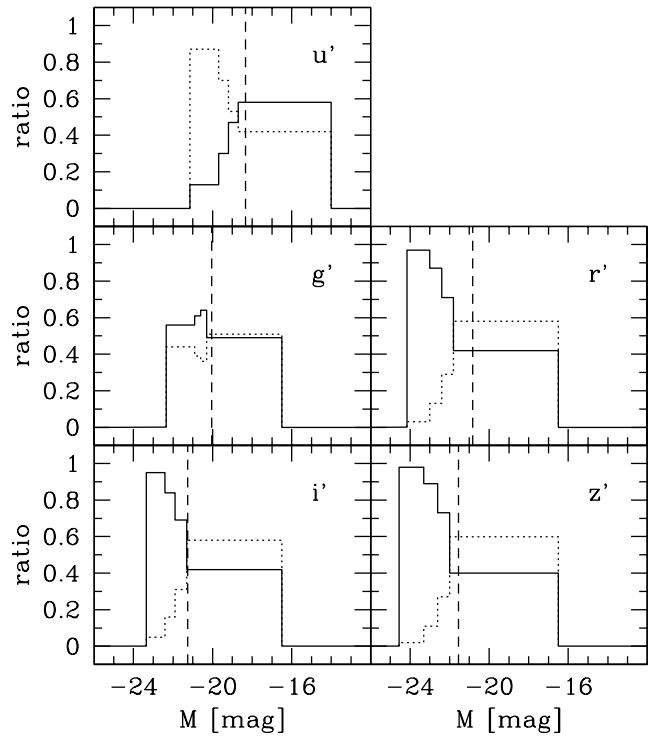

Figure 17. Fraction of early types (solid) and late types (dotted) in each of 4 luminosity bins for all 5 colors. Also shown is the magnitude of $L_\star$ galaxy (dashed).

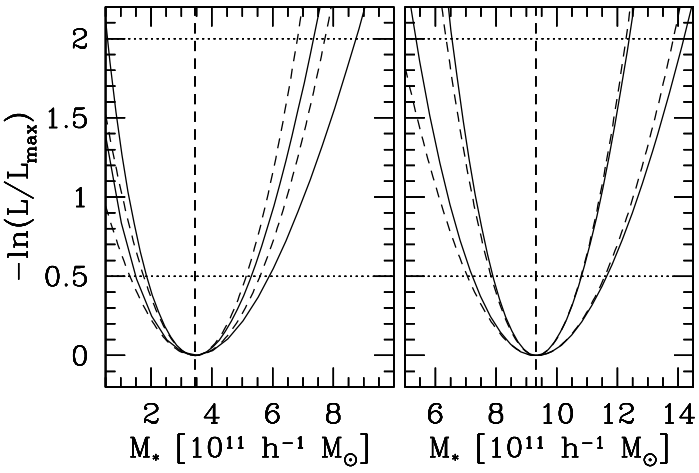

Figure 19. Comparison between exact log-likelihood (solid) and its gaussian approximation assuming rms values from the non-linear fitting routine (dashed). Left is for late type and right for early type galaxies. Narrower curves are for a fixed value of α at the minimum, while broader curves are marginalized over α. In both cases, gaussian distribution gives a good description of the error probability distribution.

ties. The main qualitative new feature of the model is that both the dark matter around the individual galaxies and dark matter in groups and clusters are included. Both components are needed to explain the observations. The two contributions have a different radial dependence and can be determined separately. This provides important constraints on the galaxy formation models, which must satisfy the relative contribution from central and group/cluster components. We also argue that correlations between the galaxy and another halo that is not the one that galaxy belongs to can be neglected, at least on scales below $1h^{-1}$Mpc of interest here.

The main result of this paper is determination of galaxy virial masses and the fraction of galaxies in groups and clusters as a function of luminosity and morphology. These provide important constraints on the galaxy formation models. The average virial mass M_{200} of an $L_\star$ galaxy is around $(5-10)\times 10^{11}h^{-1}M_\odot$, depending on the passband. This mass varies significantly with morphology and the variation is largest in u', where the difference between early and late types can be up to a factor of 10, decreasing to a factor of 2-3 in r', i' and z'. For example, in i' we find $M_{200} = (3.4\pm 2.1)\times 10^{11}h^{-1}M_\odot$ for late types and $M_{200} = (9.3\pm 2.2)\times 10^{11}h^{-1}M_\odot$ for early types. While the signal for late types is rather weak and consequently the errors are large, they are gaussian distributed and so we can exclude the possibility that in red bands the $M_\star$ for early and late types are equal.

What does this imply for the star formation efficiency as a function of galaxy morphology? To address this we first transform from i' to K band, where the luminosity is assumed to be a reliable tracer of stellar mass for a given age of the population (and IMF). This transformation does not change the results significantly, since $K-i'$ differs by 0.2-0.3 magnitudes at most between the two types (Ivezic et al. 2001). This difference is further reduced by up to 20% because of the missed light for the de-Vaucouleurs profile. As a result, the difference in M/L between the two types is reduced to a factor of 2. In K band the difference in $M_{\rm stellar}/L$ between early and late type population can be up to a factor of 2 depending on the exact ages and IMF assumed, so our results are consistent with the assumption that star formation efficiency for early and late type galaxies is the same. The errors however are still large both on the virial masses and stellar mass to light ratios and there could still be up to a factor of 2 difference. Since the current results are based on only 5% of final SDSS sample one should be able to place much better constraints on this issue in the future.

If we adopt the late(early) type stellar mass to light ratio $M_{\rm stellar}/L \sim 1.5(3)h$ in i' we find that at $L_\star$ about 10-15% of virial mass is converted to stars. The fraction of baryons inside a halo should equal Ω_b/Ω_m, which can vary between 10-20% for $\Omega_m \sim 0.3\pm 0.1$ and $\Omega_b \sim 0.04\pm 0.01$. We see that if our halo masses are correct a significant fraction of baryons, up to 100%, is converted to stars in such halos. For early types this fraction decreases with luminosity and is a factor of 2 lower at $7L_\star$. These stellar fractions can be accomodated in the standard models, but require a low matter density and/or a high baryon density, so that the overall baryon to dark matter fraction is sufficiently high.

We find that $M/L \propto L^{0.4\pm 0.2}$ in red bands (i' and z'). An increase in M/L with luminosity above $L_\star$ is expected

theoretically from semi-analytic models of galaxy formation (Kauffmann et al. 1999, Benson et al. 2000). Comparison of these results with mass tracers such as Tully-Fisher or fundamental plane is complicated, because these probe the halo at smaller radii, where the rotation velocity of dark matter could be different and where baryons could play a significant role. A detailed analysis will be presented elsewhere. The results from such analysis show that the masses obtained here are consistent with the CDM picture in which the rotation velocity drops by roughly 1.7-1.8 from the optical to the virial radius at $L_\star$. Such a drop is expected in CDM models, where the rotation curve peaks at a fraction of the virial radius and drops beyond that. However, to explain such a large drop one also needs a significant additional contribution to the rotation velocity from the stellar component and/or baryon compressed dark matter. For early types the scaling $M \propto L^{1.5}$ indicates $L \propto v_{200}^2$, while for the same galaxies the Faber-Jackson relation gives $L \propto \sigma^4$ (Bernardi et al. 2001). In this case the ratio of optical to virial circular velocity depends on luminosity and drops to 1.4 at $7L_\star$.

Comparison with other g-g lensing results is also complicated, since none of these use luminosity information, are typically at a higher redshift with poorly determined distances and may have a different morphological composition. The most direct comparison can be made to the study of early type galaxies by Wilson et al. (2001), where color information was used to determine approximate redshifts to these galaxies. A direct comparison shows that their virial mass for early type $L_\star$ galaxy is around $2 \times 10^{12} h^{-1} M_\odot$. Their sample is at a higher redshift and may not be directly comparable to ours, but the obtained value is quite close to our best fitted value of $M_\star = 2.1 \times 10^{12} h^{-1} M_\odot$ in g', which is the closest to B band used there (note that $L_\star = 1.1 \times 10^{10} h^{-2} L_\odot$ in both samples). In their analysis they assume $\beta = 0.5$, which is inconsistent with the SDSS luminosity dependent data, so their actual value of $M_\star$ could even be somewhat lower because β and $M_\star$ are anticorrelated. Earlier analysis of the dynamics of satellites around spiral galaxies gave significantly higher masses (up to a factor of 5, Zaritsky et al. 1997) and also did not show correlation between light and mass, but a more recent analysis of the SDSS data shows a better agreement with g-g lensing results (T. McKay, private communication). At the upper end of the luminosity range our results can be compared to group and cluster velocity dispersion analysis of Girardi et al. (2001). Our results agree well both on the mean luminosity of a $10^{13} h^{-1} M_\odot$ halo and on the scaling of mass with luminosity. For late type galaxies at $L_\star$ our results agree well with the virial mass derived from theoretical models by van den Bosch (2001).

There are many aspects of the analysis that could be improved upon with better statistics which will be available in the future. We mention some here. We have assumed a power law relation between mass and luminosity with a constant slope β, while theoretical models suggest β changes with mass. With the current sample the signal for galaxies less luminous than $L_\star$ is too small to be detectable and the relation between mass and luminosity cannot be established in that range. As larger samples become available this regime will be probed as well. Fraction of galaxies in groups and clusters should be determined as a function of luminosity. Similarly, galaxy morphology dependent analysis should be improved by analyzing luminosity dependence of the signal for each morphology type and by dividing the lens galaxies into several morphological classes. With better statistics the fraction of galaxies in groups and clusters could be determined as a function of luminosity and not just for the overall sample as done here. The radial distributions of dark matter and galaxies in groups and clusters as well as galaxy occupation statistics as a function of halo mass should be quantified better. These effects can change the values for $M_\star$ and β by 20-30% and remain the dominant source of systematic error. Better k-correction and evolution effects should be applied to the data to match the bright end (which receives contributions from $z \sim 0.2$) and faint end (low z) samples. This effect should not exceed 0.1-0.2 magnitudes in red bands and so should not change our conclusion on the mass luminosity relation significantly. Differences between halos of galaxies in the field and in groups and clusters could be studied in more detail, testing for example the collisionless CDM paradigm. In this paper we assumed that the profiles of galaxies within groups and halos are unchanged out to the truncation radius. In the extreme opposite case where galaxies inside groups and clusters do not retain any mass at all the virial masses of galaxies in the field will be underestimated by $1-\alpha$. This is a small correction for late type galaxies, but potentially more important for early type galaxies. Finally, the clustering correction, which corrects for the fraction of galaxies that are correlated with the lens and are not in the background, is luminosity dependent and should be done more accurately. While the procedure adopted here is reasonable, it should be studied in more detail. This effect may be removed for example if one can select background galaxies using their photometric redshift (photo z) information, although it is not clear if the faint galaxies that dominate the background population have sufficient signal to noise for this purpose. Current experience with photo z's indicates that in SDSS these work only down to $r' < 20.5$, while most of the background galaxies used for shape information are fainter than that.

As we obtain more data better statistical analysis will also be needed. Rather than divide the data in arbitrary luminosity bins, which may still be too broad for a quantitative analysis, one should parametrize the model with a few parameters and use maximum likelihood type of analysis to determine these. Photometric redshifts would also help to improve the statistics since one could weight the signal by giving optimal weight for each lens-background galaxy pair (this would then automatically downweight all the galaxies that are close to the lens). These improvements will allow one to make very robust statements on the relation between the virial mass and luminosity and on the membership in groups and clusters over a broad range of luminosities and morphological types.

US acknowledges he support of NASA, David and Lucille Packard Foundation and Alfred P. Sloan Foundation. J.G. was supported by grants 5P03D01820 and 2P03D01417 from Polish State Committee for Scientific Research. We thank Tim McKay, Erin Sheldon and Iskra Strateva for help with the interpretation of SDSS data and its analysis.

REFERENCES

Bartelmann M., Schneider P., 2001, Phys. Rep., 340, 291
Benson A. J., Cole S., Frenk C. S., Baugh C. M., Lacey C. G., 2000, MNRAS, 311, 793
Berlind A. A., Weinberg D. H., 2001, in astro-ph/0109001
Bernardi M. et al., 2001, in astro-ph/0110344
Blanton M. R. et al., 2001, AJ, 121, 2358
Brainerd T. G., Blandford R. D., Smail I., 1996, ApJ, 466, 623
Bullock J. S., Kolatt T. S., Sigad Y., Somerville R. S., Kravtsov A. V., Klypin A. A., Primack J. R., Dekel A., 2001, MNRAS, 321, 559
Dressler A., 1980, ApJ, 236, 351
Eke V. R., Navarro J. F., Steinmetz M., 2001, ApJ, 554, 114
Fischer P. et al., 2000, AJ, 120, 1198
Ghigna S., Moore B., Governato F., Lake G., Quinn T., Stadel J., 2000, ApJ, 544, 616
Girardi M., Manzato P., Mezzetti M., Giuricin G., Limboz F., 2001, in astro-ph/0112534
Guzik J., Seljak U. ., 2001, MNRAS, 321, 439
Hoekstra H., Franx M., Kuijken K., van Dokkum P. G., 2001, in astro-ph/0109445
Hudson M. J., Gwyn S. D. J., Dahle H., Kaiser N., 1998, ApJ, 503, 531
Ivezic Z. et al., 2001, in astro-ph/0111024
Jenkins A., Frenk C. S., White S. D. M., Colberg J. M., Cole S., Evrard A. E., Couchman H. M. P., Yoshida N., 2001, MNRAS, 321, 372
Jing Y. P., Mo H. J., Boerner G., 1998, ApJ, 494, 1
Kauffmann G., Colberg J. M., Diaferio A., White S. D. M., 1999, MNRAS, 303, 188
Klypin A., Kravtsov A. V., Bullock J. S., Primack J. R., 2001, ApJ, 554, 903
Lilly S. J., Le Fevre O., Crampton D., Hammer F., Tresse L., 1995, ApJ, 455, 50
McKay T. A. et al., 2001, in astro-ph/0108013
Navarro J. F., Frenk C. S., White S. D. M., 1997, ApJ, 490, 493
Peacock J. A., Smith R. E., 2000, MNRAS, 318, 1144
Scoccimarro R., Sheth R. K., Hui L., Jain B., 2001, ApJ, 546, 20
Seljak U., 2000, MNRAS, 318, 203
Sheth R. K., Mo H. J., Tormen G., 2001, MNRAS, 323, 1
Sheth R. K., Tormen G., 1999, MNRAS, 308, 119
Smith D. R., Bernstein G. M., Fischer P., Jarvis M., 2001, ApJ, 551, 643
Somerville R. S., Primack J. R., 1999, MNRAS, 310, 1087
Spergel D. N., Steinhardt P. J., 2000, Physical Review Letters, 84, 3760
Springel V., White S. D. M., Tormen G., Kauffmann G., 2001, MNRAS, 328, 726
Strateva I., Ivezic Z., Knapp G. R., Narayanan V. K., Strauss M. A., et al. , 2001, in astro-ph/0107201
Tyson J. A., Valdes F., Jarvis J. F., Mills A. P., 1984, ApJ, 281, L59
van den Bosch F. C., 2001, in astro-ph/0112566
White M., Hernquist L., Springel V., 2001, in astro-ph/0107023
Wilson G., Kaiser N., Luppino G. A., Cowie L. L., 2001, ApJ, 555, 572
Zaritsky D., Smith R., Frenk C., White S. D. M., 1997, ApJ, 478, 39

band	$M_\star[10^{11}h^{-1}M_\odot]$	β	α	$R_{M_\star\beta}$	$L_\star[10^{10}h^{-2}L_\odot]$
u'	8.05±1.23	0.23±0.22	0.23±0.03	-0.04	0.78±0.06
g'	10.24±1.62	1.67±0.22	0.20±0.03	-0.71	1.11±0.04
r'	8.96±1.59	1.51±0.16	0.17±0.03	-0.83	1.51±0.04
i'	8.54±1.53	1.51±0.14	0.17±0.03	-0.85	2.05±0.08
z'	10.01±1.66	1.44±0.13	0.16±0.03	-0.83	2.58±0.10
u'	6.16±1.70	-0.52±0.29	0.15±0.02	0.83	0.78±0.06
g'	9.33±1.58	1.16±0.23	0.17±0.02	-0.35	1.11±0.04
r'	7.56±1.55	1.34±0.17	0.18±0.03	-0.72	1.51±0.04
i'	7.16±1.53	1.40±0.15	0.17±0.03	-0.79	2.05±0.08
z'	8.08±1.62	1.35±0.14	0.17±0.03	-0.75	2.58±0.10

Table 1. Best fitted parameters to the SDSS data in five colors assuming $\alpha = 0$ for all but the faintest bin. The corresponding values for $M_\star$ using equal α for all bins are 10-20% lower, while the other parameters do not change much. Also given is the correlation coefficient between M_* and β and the value of $L_\star$.

band	type	$M_\star$ $[10^{11}h^{-1}M_\odot]$	α	$L_\star[10^{10}h^{-2}L_\odot]$
u'	E	25.55±5.78	0.31±0.07	0.78±0.06
u'	S	2.52±1.58	0.09±0.04	0.78±0.06
g'	E	21.94±5.25	0.29±0.07	1.11±0.04
g'	S	3.18±2.02	0.08±0.05	1.11±0.04
r'	E	10.73±2.53	0.28±0.08	1.51±0.04
r'	S	3.26±2.08	0.08±0.05	1.51±0.04
i'	E	9.32±2.26	0.28±0.08	2.05±0.08
i'	S	3.44±2.14	0.08±0.05	2.05±0.08
z'	E	10.06±2.38	0.28±0.08	2.58±0.10
z'	S	4.08±2.63	0.08±0.05	2.58±0.10

Table 2. Best fitted parameters for early type (E) and late type (S) galaxies as a function of color. Early types have higher $M_\star$ and group/cluster fraction than late types.